JOURNAL OF THE ROYAL SOCIETY Interface

Healing substrates with mobile, particle-filled microcapsules: designing a 'repair and go' system

Rolf Verberg, Alex T Dale, Prashant Kumar, Alexander Alexeev and Anna C Balazs

J. R. Soc. Interface 2007 **4**, 349-357
doi: 10.1098/rsif.2006.0165

JOURNAL OF THE ROYAL SOCIETY Interface

J. R. Soc. Interface (2007) **4**, 349–357
doi:10.1098/rsif.2006.0165
Published online 3 October 2006

Healing substrates with mobile, particle-filled microcapsules: designing a 'repair and go' system

Rolf Verberg, Alex T. Dale, Prashant Kumar, Alexander Alexeev and Anna C. Balazs*

Department of Chemical Engineering, University of Pittsburgh, Pittsburgh, PA 15261, USA

We model the rolling motion of a fluid-driven, particle-filled microcapsule along a heterogeneous, adhesive substrate to determine how the release of the encapsulated nanoparticles can be harnessed to repair damage on the underlying surface. We integrate the lattice Boltzmann model for hydrodynamics and the lattice spring model for the micromechanics of elastic solids to capture the interactions between the elastic shell of the microcapsule and the surrounding fluids. A Brownian dynamics model is used to simulate the release of nanoparticles from the capsule and their diffusion into the surrounding solution. We focus on a substrate that contains a damaged region (e.g. a crack or eroded surface coating), which prevents the otherwise mobile capsule from rolling along the surface. We isolate conditions where nanoparticles released from the arrested capsule can repair the damage and thereby enable the capsules to again move along the substrate. Through these studies, we establish guidelines for designing particle-filled microcapsules that perform a 'repair and go' function and thus, can be utilized to repair damage in microchannels and microfluidic devices.

Keywords: computer simulations; microcapsules; nanoparticles; substrate-healing

1. INTRODUCTION

In biological wound healing, or self-repair, the circulatory system transports vital cells to the injured site. One potential means of introducing self-repair in synthetic systems is to embed artificial circulatory networks into the materials. This synthetic vasculature would encompass a network of fluid-filled microchannels (Therriault *et al.* 2005), which could be harnessed to deliver the healing agents to specific locations within the system. Instead of simply streaming the healing reagents in the channels, it might be more advantageous to encapsulate these reagents in porous microcapsules, which could serve as artificial cells or 'synthetic leukocytes'. In particular, the appropriately designed microcapsules would not only 'sense' the state of the system, but also direct the vital healing components specifically to the damaged sites.

Herein, we use computational modelling to design microcapsules that could act as 'artificial leukocytes'. We focus on microcapsules that are driven by an imposed flow to move along an adhesive surface, which represents the wall of a microchannel (either in the synthetic microvasculature, or more generally, in a microfluidic device). The microcapsules enclose a solution of nanoparticles and these nanoparticles can diffuse from the interior of the capsule into the host fluid. Our aim is to isolate conditions where the microcapsule becomes localized at a damaged site on the surface and, thus, preferentially deposits a significant fraction of the nanoparticles onto this region. In this manner, the particles could be harnessed to fill nanoscale cracks or repave the surface with a coating that has been eroded or worn away. Once the nanoparticles have effectively mended the damage, the microcapsules could traverse the region and move further along the surface, where they could potentially sense and repair other injuries. In effect, the microcapsules could be tailored to provide a 'repair and go' function.

In addition to facilitating the design of 'artificial leukocytes', these studies can enhance our understanding of targeted delivery from particle-filled microcapsules. Recently, there has been significant interest in the encapsulation of nanoparticles into microscale 'carriers'. These microcarriers or capsules provide a means of regulating the rate of release of the enclosed nanoparticles and, thus, controlling the incorporation of the particles into the system (Donbrow 1992). The carriers also facilitate handling, provide protection and enhance storage stability; these features are particularly important if the nanoparticles are catalysts or other reactive species. Once released into the host material, the nanoparticles can impart

*Author for correspondence (balazs1@engr.pitt.edu).

One contribution of 9 to a themed supplement 'Self-healing polymers and composites'.

Received 22 August 2006
Accepted 15 September 2006

characteristics that range from novel optical, electromagnetic and mechanical properties, to aesthetic attributes, such as specified colour or fragrance. Consequently, the nanoparticle-filled microcarriers could ultimately be utilized in the fabrication of a tremendous array of materials, including inks, paints, pharmaceuticals, personal care products, foods and robust composites.

Despite the potential utility of these assemblies in a number of industries, there have been few systematic studies to probe the release of encapsulated nanoparticles on the single capsule level and to isolate the factors that control the release and dispersion of the particles (Skirtach *et al.* 2005). Prior studies were mainly focused on nanoparticle/capsule assemblies for controlled drug release (Donbrow 1992; Ai *et al.* 2003; Skirtach *et al.* 2005; Sukhorukov *et al.* 2005). But new types of nanoparticles that display a range of novel compositions and structure are now being fabricated at a distinctly rapid pace (Whitesides & Wong 2006). These recent experimental developments open up the possibility of harnessing the controlled nanoparticle release in a host of materials and a range of novel applications.

To carry out this computational study of the release of nanoparticles from a mobile microcapsule, we take the advantage of our recently developed hybrid 'LBM/LSM' technique (Alexeev *et al.* 2005, 2006; Buxton *et al.* 2005); here, the capsule's shell is modelled through the lattice spring model (LSM) for the micromechanics of elastic solids, and the dynamic behaviour of the encapsulated and external host fluids is captured through the lattice Boltzmann model (LBM) for hydrodynamics. The two systems interact through appropriate boundary conditions at the solid–fluid interface. Using this LBM/LSM, we can capture the complex fluid–structure interactions in this system. We couple the LSM/LBM to a Brownian dynamics model (BDM) for the nanoparticles to simulate the diffusion of the particles from the interior of the fluid-filled capsule through the elastic shell to the host solution. Below, we provide a brief description of our LBM, LSM and BDM and then, explain the boundary conditions that link these different components of the method. We also detail the boundary conditions that are used to distinguish the intact surface from the damaged regions of the substrate.

2. METHODOLOGY

2.1. Computational approaches

The lattice Boltzmann model (Succi 2001) is a lattice-based method for simulating hydrodynamic flows. Unlike conventional numerical schemes, which involve a direct discretization of the continuum equations, the LBM incorporates the mesoscopic physics of fluid 'particles' propagating and colliding on a simple lattice such that the averaged, macroscopic properties of the system obey the Navier–Stokes equations (Succi 2001). Specifically, the model consists of two processes, the first being the propagation of fluid particles to neighbouring lattice sites, and the second being the collisions between particles when they reach a site. For a single component fluid, the system is characterized by a single-particle velocity distribution function, $f(\boldsymbol{r}, \boldsymbol{c}_i, t)$, describing the mass density of fluid particles with velocity $\boldsymbol{c}_i$ at a lattice node $\boldsymbol{r}$ at time t. Here, $\boldsymbol{c}_i$, $\boldsymbol{r}$ and t are discrete variables, while the distribution function itself is a continuous variable. The hydrodynamic quantities of interest, namely the mass density, the momentum density and the momentum flux, are calculated as moments of the distribution function.

The computational efficiency of the approach stems from the fact that only a small set of velocities is necessary to effectively simulate the Navier–Stokes equation. In two dimensions, we use nine velocities, which correspond to movement to the nearest and the next-nearest neighbour directions of a square lattice and to rest particles. The magnitudes of these velocities are such that fluid particles propagate from one lattice site to the next in exactly one time-step. (All the variables are expressed in terms of the time-step Δt and the lattice spacing Δx; in our simulations, both Δt and Δx are set equal to 1).

Similar to the LBM, the rules of the lattice spring model (LSM) capture microscopic phenomena, whose emergent behaviour captures the macroscopic properties of the system. In particular, the LSM is adopted from atomistic models of solid-state and molecular physics (Ashurst & Hoover 1976), and involves a network of interconnected 'springs', which describe the interactions between neighbouring units. The large-scale behaviour of the resultant system can be mapped onto continuum elasticity theory (Buxton *et al.* 2001).

Within this model, the network of harmonic springs, which connect regularly spaced mass points or nodes, give rise to a spring force $\boldsymbol{F}_\mathrm{s}$ on node $\boldsymbol{r}_i$ of the form (Alexeev *et al.* 2005)

$$\boldsymbol{F}_\mathrm{s}(\boldsymbol{r}_i) = -\sum_j k_{ij}\left[\frac{\left(r_{ij} - r_{ij}^{\mathrm{eq}}\right)}{r_{ij}}\right]\boldsymbol{r}_{ij}, \qquad (2.1)$$

with $\boldsymbol{r}_{ij} = \boldsymbol{r}_i - \boldsymbol{r}_j$ and $r_{ij} = \|\boldsymbol{r}_{ij}\|$. The parameter r_{ij}^{eq} is the equilibrium length of the spring that connects nodes $\boldsymbol{r}_i$ and $\boldsymbol{r}_j$, and k_{ij} is the corresponding spring constant. The dynamic behaviour of the solid material is described by Newton's equation of motion, $\boldsymbol{F}(\boldsymbol{r}_i) = M_i(\mathrm{d}^2\boldsymbol{r}_i/\mathrm{d}t^2)$, where $\boldsymbol{F}$ is the total force acting on the node $\boldsymbol{r}_i$, and M_i is the mass at node $\boldsymbol{r}_i$. (Within this equation, we can introduce a friction term to account for dissipation.) This total force consists of the spring force obtained from equation (2.1), the force exerted by the fluid on the solid at the solid–fluid boundary, and external forces, such as gravity or the adhesion force that we introduce later. We use the Verlet algorithm to integrate Newton's equation of motion. This is a well-known molecular dynamics algorithm that updates the positions, velocities and accelerations of each node in discrete time-steps (Tuckerman *et al.* 1992).

To capture the interaction between the solids and the fluids, the velocities of lattice spring nodes situated at the solid–fluid interface are transmitted to the surrounding fluids. In turn, these LSM nodes experience

forces due to the fluid pressure and viscous stresses at the interface. In our current implementation, fluid particles that are moving on a link, which intersects the solid–fluid interface are bounced back into the fluid phase at the intersection point, according to the scheme developed by Bouzidi *et al.* (2001). This implementation gives a no-slip boundary condition at the solid–fluid interface, with errors that are of second-order accuracy in the spatial discretization. As a result of the bounce back process, the fluid exerts a force on the solid–fluid interface. This force is taken to be equal to the rate of exchange in momentum that takes place, as the fluid particles are reflected at the interface; it is applied as a load to the neighbouring LSM nodes (Alexeev *et al.* 2005).

At the start of the simulation, a fixed number of nanoparticles are introduced into the fluid-filled interior of the microcapsule. The nanoparticles are modelled as point particles; since their mass is small, their motion is in the so-called 'over-damped' regime. Consequently, their velocity is dictated by the local fluid velocity. The particles can diffuse within the encapsulated fluid, the elastic shell and the external, host solution. In particular, the nanoparticles travel along trajectories that obey a stochastic differential equation (Ottinger 1996; Verberg *et al.* 2005; the operative equation of a BDM),

$$\mathrm{d}\boldsymbol{r}(t) = \boldsymbol{u}(\boldsymbol{r}, t)\mathrm{d}t + \sqrt{2D_0}\mathrm{d}\boldsymbol{W}(t). \tag{2.2}$$

The first term gives the advection owing to the local fluid velocity $\boldsymbol{u}(\boldsymbol{r}, t)$. The second term is the Brownian contribution, with D_0 being the particles' diffusion coefficient and $\mathrm{d}\boldsymbol{W}(t)$ being the differential of a Wiener process with unit variance. We specify a value $D_0 = D_\mathrm{f}$ in the fluids. The shell of our microcapsule is assumed to be permeable to the nanoparticles (i.e. it represents a porous polymeric material) and within this region, the particles have an effective diffusion coefficient $D_0 = D_\mathrm{s}$. Note that the volume of the capsule is assumed to remain constant and the encapsulated and external fluids are taken to be identical single-component liquids, which have the same viscosity and density. In this study, we neglect interactions between the particles, as well as 'backflow' effects (the impact of the particles' motion on the flow field). This approximation is appropriate for dissolved components or sub-micrometre sized particles at a relatively low concentration (as is the case for the nanoparticles released into the host solution).

We use an Euler method to solve equation (2.2),

$$\boldsymbol{r}(t + \Delta t) = \boldsymbol{r}(t) + \boldsymbol{u}[\boldsymbol{r}(t)]\Delta t + \sqrt{2D_0}\Delta\boldsymbol{W}(t), \tag{2.3}$$

where the increment $\Delta\boldsymbol{W}$ is sampled randomly from a truncated Gaussian distribution with variance $2\Delta t$ (in two dimensions). The fluid velocity at the particle position is obtained directly from the velocities at the LBM nodes by using bilinear interpolation (Verberg *et al.* submitted); it is in this manner that the dynamics of the fluid and the nanoparticles are coupled. The time-step is identical to that for the LBM part of the algorithm, i.e. $\Delta t = 1$.

Finally, we note that taking an ensemble average of the particle trajectories obtained form equation (2.3) is equivalent to solving the convection–diffusion equation for the number concentration $c(\boldsymbol{r}, t)$of the nanoparticles (Ottinger 1996), i.e.

$$\frac{\partial c}{\partial t} + \boldsymbol{u}\cdot\nabla c = D_0\nabla^2 c. \tag{2.4}$$

2.2. Modelling the particle–wall interactions

Our simulation involves two types of surface regions: one region where the wall or the surface coating is perfectly intact, and a second region where this surface has sustained damage or the coating has been eroded away. We assume that the chemical nature of the intact and the damaged regions is different, as would be the case, for example, where the erosion of the coating has exposed a chemically distinct sublayer. Thus, the capsule and the released particles interact with the undamaged and the damaged regions in distinctly different ways. Here, we describe the interactions between the released particles and the different surface regions. In the next section, we discuss the interaction between the capsule and the substrate.

In the undamaged region, we implement the boundary conditions for a non-interacting wall (Szymczak & Ladd 2003), i.e. $\boldsymbol{n}(\boldsymbol{r})\cdot\nabla c(\boldsymbol{r}, t)|_\mathrm{surface} = 0$, with $\boldsymbol{n}(\boldsymbol{r})$ being the unit vector normal to the surface. In this case, the particles simply undergo specular reflection at the solid–fluid interface.

Within the damaged region, we implement a boundary condition that is appropriate for the chemisorption of particles (Szymczak & Ladd 2003). In this scenario, the adsorption is limited to a single monolayer of particles. We note that this constraint also models situations where the reaction with the substrate is limited to a certain number of 'active sites'. The boundary condition for chemisorption is a special case of the general mass-transfer boundary condition,

$$-D_0\boldsymbol{n}\cdot\nabla c|_\mathrm{surface} = f(c_\mathrm{s}), \tag{2.5}$$

where $f(c_\mathrm{s})$ is the flux of particles that enter or leave the fluid (with $f<0$ for particle deposition). To the lowest order, $f(c_\mathrm{s})$ can be modelled by a linear kinetic law (Szymczak & Ladd 2003),

$$f(c_\mathrm{s}) = -k(1-\Theta)c_\mathrm{s}. \tag{2.6}$$

Here, the reaction rate is proportional to the concentration of nanoparticles at the surface, $c_\mathrm{s} \equiv c(\mathbf{r}, t)|_\mathrm{surface}$, with the proportionality constant being the product of a reaction constant k and the fraction $(1-\Theta(\boldsymbol{r},t))$ of the surface area that is 'empty' or 'available' to the nanoparticles; thus, $\Theta(\boldsymbol{r},t)$ is the fractional coverage of the surface by the nanoparticles. The case of $\Theta = 1$ represents a surface where all the active sites are occupied by nanoparticles, yielding a non-reactive substrate. On the other hand, $\Theta = 0$ characterizes a completely empty surface.

One way to implement the above boundary conditions would be to remove particles from the system when their trajectories intersect the wall, such that the emerging concentration field obeys equations

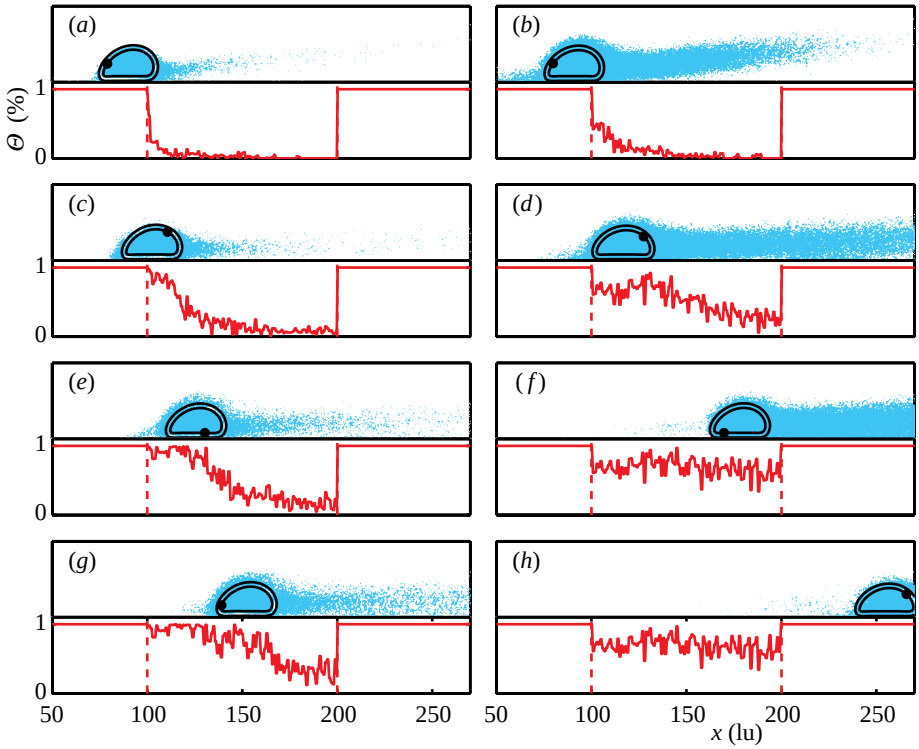

Figure 1. Snapshots of the simulation at regular time-intervals for a slow release rate (a,c,e,g $D_s/D_f=0.0002$) and a high release rate (b,d,f,g $D_s/D_f=0.08$) for $\Phi=4.1$ and $Pe=161$: (a,b) $t=8400$, (c,d) $t=13\,400$, (e,f) $t=18\,400$, and (g,h) $t=23\,400$ (all in lattice units). The nanoparticles are drawn as blue dots. The capsule's shell is bounded by the outer and inner black lines. The solid black dot is added to reveal the rotation of the shell. The solid red curve shows the fractional occupation, Θ, of the substrate as a function of x (in lattice units). The dashed red lines mark the two edges of the initially damaged region.

(2.5) and (2.6). However, it is computationally more convenient to specularly reflect particles whose trajectories intersect the wall and to inject new 'holes' or particles with negative mass, such that the net flux across the wall obeys equations (2.5) and (2.6). Hence, our actual implementation of the above boundary conditions consists of the following five steps (Szymczak & Ladd 2003). First, we divide the entire solid surface into a number of cells with area ΔS_i (with each ΔS_i being half a lattice site). Second, we calculate the concentration $c_s(\boldsymbol{r}_i)$ of nanoparticles at the centre of each of these cells, $\boldsymbol{r}_i$, and calculate the flux $f(c_s)$ from equations (2.5) and (2.6). (Note that holes in the bulk count towards the local concentration as particles with negative mass.) Third, we distribute $f(c_s)$ new holes at random positions within the surface element ΔS_i. Fourth, we advance these injected holes according to equation (2.3) with a time-step that is picked randomly from a uniform distribution in the range $[0, \Delta t]$. Finally, we increment the surface coverage Θ at position $\boldsymbol{r}_i$ with an amount $f(c_s)$ to account for the particle deposition.

After their injection, the holes follow trajectories that are calculated just like those for the regular particles. Hence, except for the time-step during which they are injected, the holes are advanced according to equation (2.3) with a time-step Δt, using specular reflection at the solid surfaces. As mentioned earlier, the holes count towards the local concentration as particles with negative mass. Note that an undamaged ($\Theta=1$) surface indeed leads to $f(c_s)=0$, i.e. $\boldsymbol{n}(\boldsymbol{r})\cdot\nabla c(r,t)|_{\text{surface}}=0$, which is the boundary condition for a non-interacting wall, as discussed earlier.

2.3. Modelling the capsule–wall interactions

A crucial aspect of the fluid-driven motion of compliant microcapsules is that the capsules exhibit a lift force in the presence of gradients in the local flow velocity. In particular, gradients in the flow field will distort the capsule such that it becomes elongated and tilted with respect to the mean flow direction. For pressure-driven channel flow, this leads to a lift force that tends to drive the capsules away from the channel walls. The resulting increased distance between capsules and wall severely reduces the effectiveness of the delivery of nanoparticles to the substrate (Verberg *et al.* submitted). To overcome this limitation, we study the case where the microcapsules exhibit an adhesive interaction with the substrate. This adhesive interaction keeps the capsules rolling along the wall, as long as the total adhesion force is sufficiently large to balance the lift force.

In our simulation, this adhesive interaction is modelled via a non-specific Morse potential (Alexeev *et al.* 2005),

$$\phi(r)=\varepsilon\left(1-\exp\left[-\frac{(r-r_0)}{\kappa}\right]\right)^2. \qquad (2.7)$$

Here, ε and κ characterize the respective strength and range of the interaction potential. The value r represents the distance between a lattice spring node

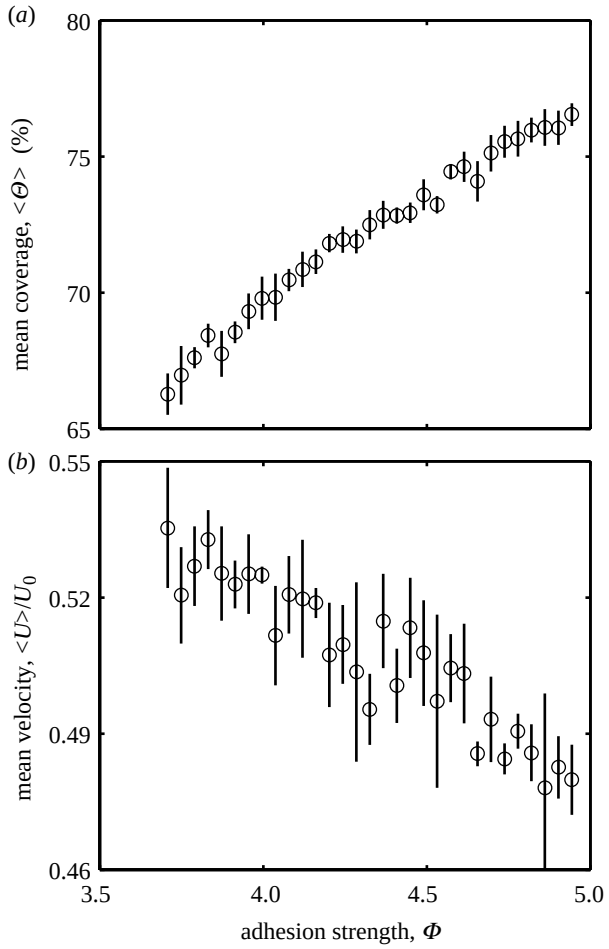

Figure 2. (*a*) Mean surface coverage, $\langle\Theta\rangle$, (in %) and (*b*) mean relative capsule velocity, $\langle U\rangle/U_0$, as a function of the dimensionless adhesion strength, Φ, for $Pe=161$ and $D_s/D_f=0.04$. The data points are the averaged values and the error bars are the standard deviations for four simulations with different random number sequences in the Brownian dynamics simulation and otherwise identical parameters.

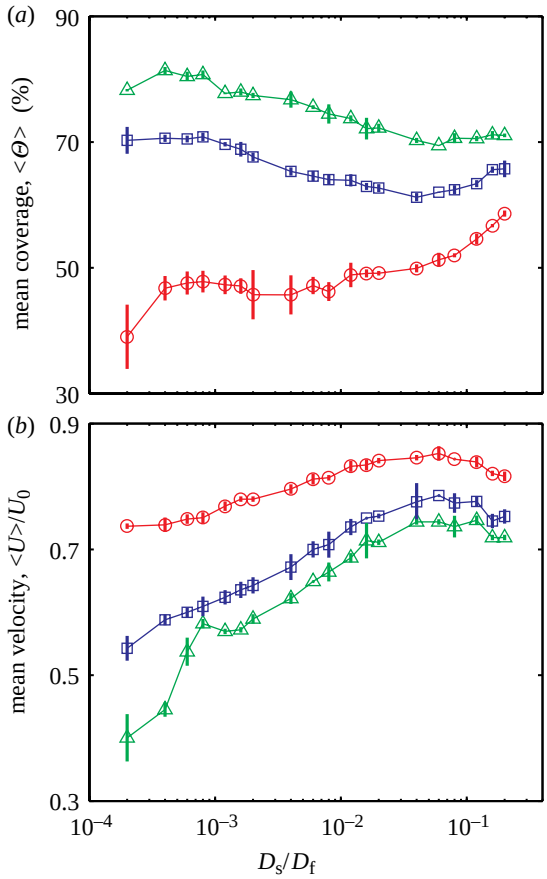

Figure 3. (*a*) Mean surface coverage, $\langle\Theta\rangle$, (in %) and (*b*) mean relative capsule velocity, $\langle U\rangle/U_0$, as a function of D_s/D_f for three dimensionless adhesion strengths: $\Phi=2.5$ (circles), $\Phi=3.3$ (squares) and $\Phi=4.1$ (triangles); the Peclet number is fixed at 161. The data points and the error bars are the averaged values and the standard deviations for three individual simulations as shown in figure 2. The lines through the points serve as a guide to the eye.

on the capsule's outer surface and the centre $\boldsymbol{r}_i$ of each surface element ΔS_i; r_0 is the distance where this force is equal to zero. In all our simulations, we set $\kappa=1$ and $r_0=1$, while ε depends on the level of damage as discussed later.

We assume that the microcapsule experiences a different interaction with the intact and the damaged region of the surface. For example, as mentioned earlier, the damage could expose a chemically distinct sublayer, which modifies the adhesive interaction between the capsule and the substrate. To model this aspect, we assume that the strength of the adhesive interaction is proportional to the fractional surface coverage, i.e.

$$\varepsilon = \varepsilon_0\Theta, \tag{2.8}$$

with ε_0 being the adhesive strength for the intact surface. In other words, the capsules can only adhere to surfaces that have been paved to some extent by the released nanoparticles.

While an imposed pressure gradient drives the capsule to move along the surface, the capsule can get 'stuck' at the edge of the damaged area. In particular, if $\Theta \ll 1$, then $\varepsilon \ll \varepsilon_0$ in the damaged area and there is a strong gradient in the adhesion force along the substrate; this leads to a force that counteracts the imposed pressure gradient. After a significant fraction of released nanoparticles have reacted with the damaged area, the value of Θ increases; this in turn increases the adhesive strength and allows the capsule to continue its motion along the surface. In effect, the adsorbed particles alter the physical characteristics or wetting properties of the damaged region and thereby modify the motion of capsules past the damaged region.

We note that the above scenario could be achieved in a number of ways. For example, the damaged region can represent a shallow notch or scratch, which the capsules cannot readily traverse until this fissure is filled with the nanoparticles. In another possible scenario, the *A*-like outer layer of the capsule is chemically incompatible with the exposed *B*-like sublayer of the damaged region. If the particles are coated with a *C*-like compatibilizer, then the released particles will cover the *B* domain. This will lower the interfacial energy within the system and thus promote the passage of the capsules over the damaged area. More specifically, if we consider the microcapsules and the adhesive coating to be hydrophilic, then the ideal particles could be Janus beads (Perro *et al.* 2005), which are half hydrophobic and half hydrophilic, or

hydrophilic particles with a low surface coverage of labile hydrophobic ligands, which become localized in one region when they come in contact with the hydrophobic surface (Kim *et al.* 2006). In both scenarios, one portion of the particles would bind to the hydrophobic substrate and the hydrophilic 'face' would be exposed to the fluid. With the hydrophilic coating now in tact, the capsule could once again be driven by the imposed flow to move along the surface.

3. RESULTS AND DISCUSSION

We focus on particle-filled microcapsules that are propelled through a straight, two-dimensional channel by a constant imposed pressure gradient $\nabla_x P = 2\times10^{-5}$, which is introduced in the LBM through a uniform body force (Succi 2001). Periodic boundary conditions are applied in the flow (x)-direction. Both the top and the bottom wall are held stationary. The top wall is fully intact (i.e. non-interacting at all times), while the bottom wall serves as our substrate. The length of our simulation box in the flow direction is $L=300$, while the height of the channel is $H=60$. Note that all the values are expressed in lattice Boltzmann units.

In all our calculations, the shell of the capsule consists of two concentric layers, each containing $N=40$ lattice spring nodes. We set the outer radius of the undeformed capsule to $R=10$; this choice gives a separation between the LSM nodes of $\Delta r \approx 1.5$ and a shell thickness of $h=\Delta r \approx 1.5$. The Young modulus of the shell is held fixed at $E=1/3$. In all the simulations described herein, we set the density, ρ, of the elastic shell, the external fluid and the encapsulated fluid equal to one, while the viscosity of the fluids is fixed at $\mu=1/6$. At the onset of the simulation, $N_\mathrm{p}=1\times10^5$ nanoparticles are inserted into the interior of the capsule. Prior to starting each simulation run, the positions of the nanoparticles are equilibrated, such that they are uniformly distributed throughout the encapsulated fluid.

The substrate is divided into a damaged region (between $x=100$ and $x=200$) and an intact region (everywhere else), i.e. $\Theta(x,y=0,t=0)=0$ for $100<x<200$, while $\Theta(x,\, y=0,\, t=0)=1$ for $x\leq100$ and $x\geq200$. Initially, a capsule rolls along the intact surface, where the capsule–surface interaction is given by equation (2.7) with $\varepsilon=\varepsilon_0$. Since the surface coverage in the damaged region is initially zero, there is no adhesive interaction between the capsule and the damaged area at the onset of the simulation.

In terms of dimensionless numbers, we can characterize the motion of a capsule along a substrate by the Reynolds number $Re=\rho U_0 R/\mu$, where U_0 is the centre of mass velocity of the capsule along the undamaged portion of the substrate. The Reynolds number characterizes the relative importance of the inertial and viscous effects. All our simulations are limited to low Reynolds number flow, where the influence of inertial effects can be neglected.

We also specify a dimensionless interaction strength $\Phi=\varepsilon N/Eh\kappa^2$, which represents the ratio of the interaction strength to the membrane stiffness. For $\Phi\gg1$, this interaction leads to significant deformation of the capsule, while for $\Phi\ll1$, the effect is small. The interaction strength initially has a value of zero for the completely damaged substrate, and increases as the surface is repaired, with its maximum value being the same as that for the undamaged region of the substrate.

The motion of the nanoparticles can be characterized by the Peclet number, $Pe=U_0H/D_\mathrm{f}$, which represents the importance of convection relative to that of diffusion. A low Peclet number indicates a situation where diffusion dominates the motion of the nanoparticles and, conversely, a high Peclet number indicates a scenario where convection dominates, i.e. where the nanoparticles mostly follow the streamlines in the fluid, with only a little deviation due to diffusion.

We can relate the above simulation parameters to experimental values by considering microcapsules that are created by a layer-by-layer (LBL) deposition method (Fery *et al.* 2004; Vinogradova 2004) and are propelled by an aqueous solution, whose viscosity is $\mu\approx10^{-3}$ kg s^{-1} m^{-1} and density is $\rho\approx10^3$ kg m^{-3}. For LBL microcapsules, the elasticity of the shell is of the order of 0.1–1 Gpa, and these elastic properties are found to be independent of the speed of deformation (Dubreuil *et al.* 2003; Elsner *et al.* 2004; Fery *et al.* 2004). (We note that the Young modulus of the membrane can be tailored by varying the salt concentration in the solution or the solvent temperature.) An experimentally realistic value of the membrane thickness h is *ca* 50 nm and the capsule size can be of the order of tens of micrometres (Fery *et al.* 2004; Vinogradova 2004).

A polyelectrolyte coating on the substrate can be utilized to produce an adhesive interaction between the microcapsule and the substrate. The total adhesion energy can be estimated to be of the order of $w\sim10^{-14}$ J per capsule (Nolte & Fery 2004), while the interaction range is roughly $\kappa\sim10^{-8}$–10^{-7} m (Bosio *et al.* 2004). To obtain an estimate for $\Phi=\varepsilon N/Eh\kappa^2$, we set w equal to εN and take Eh from the example above (0.1–1 Gpa$\times$ 50 nm). We then find that Φ is of the same order of magnitude considered in the simulations, i.e. of the order of unity. Moreover, the experiments show that the adhesion interaction can be tuned by varying the thickness of the capsule wall.

In figure 1, we illustrate the graphical output from the simulation for a relatively low and a relatively high value of D_s. The nanoparticles are drawn as blue dots and the swath of blue outside the capsule reveals the extent to which the particles are dispersed in the solution. The capsule's shell is bounded by the outer and the inner black lines. The solid black dot is added to reveal the rotation of the shell. The solid red curve shows the fractional occupation, Θ, of the substrate as a function of x (varying between one for the intact region and zero for the damaged region). The dotted red lines mark the two edges of the initially damaged region. At the onset, this region is devoid of nanoparticles; however, over time, a fraction of the released nanoparticles adsorb onto this surface, as can be seen in the series of snapshots. In particular, each discrete site can absorb up to 100 particles. This number, in combination with the total number N_p of nanoparticles at the onset of the simulation, was chosen to minimize the error in the results due to

statistical fluctuations. (Once a site is full, the walls become non-interactive and particles are simply specularly reflected back into fluid.)

The strength of the adhesive interaction between the capsule and the substrate is found to have a significant effect on both the average velocity of the capsule and the final mean surface coverage in the damaged region, as can be seen in figure 2. Here, the adhesion strength is varied by altering the value of ε_0 from 0.045 ($\Phi=3.7$) to 0.06 ($\Phi=4.9$). We calculate the mean centre of mass velocity, $\langle U\rangle$, of the capsule within the damaged region from the horizontal components of the velocities of the capsule's lattice spring nodes. Note that the mean capsule velocity in the damaged region is normalized by the capsule velocity along an undamaged surface, U_0, for the same flow conditions. Increasing the adhesive interaction counteracts the effects of the imposed pressure gradient and reduces the capsule's velocity.

The mean surface coverage, $\langle\Theta\rangle$, is obtained by summing the fractional coverage at each site in the initially damaged area and dividing the result by the number of sites in this area. Here, the surface coverage is calculated after it has reached its steady-state profile, i.e. well after the capsule has traversed the entire damaged region. The decrease in the average velocity with increasing Φ means that the capsule spends more time localized within the damaged region for larger Φ. This in turn means that the particles are preferentially released within this region, thus contributing to the higher surface coverage (figure 2).

Another critical parameter that controls the efficiency of the assembly in repairing the surface is D_s. Since the capsule's shell represents a porous polymeric material, the diffusion of the nanoparticles through this layer will be slower than that through the fluid phases. Thus, the diffusion through the shell will control the release rate of the nanoparticles. To grasp the importance of the particle diffusion through the shell, we systematically varied D_s relative to D_f. In figure 3, we summarize the results for the final mean surface coverage, $\langle\Theta\rangle$, and the mean relative capsule velocity, $\langle U\rangle/U_0$, as a function of D_s/D_f for various values of the adhesive interaction strength, Φ. Note that the mean surface coverage is again calculated after the capsule has travelled over the entire damaged region and the coverage profile has reached its final steady state. Overall, we find that increasing Φ at all values of D_s/D_f leads to higher surface coverage and lower mean velocity, as shown in figure 2. The trends for a fixed Φ and varying D_s/D_f, however, reveal more subtle and intriguing behaviour within the system.

We first focus on the case of the highest adhesive strength ($\Phi=4.1$), where increases in D_s lead to both a decrease in surface coverage and an increase in the relative velocity of the capsule in the damaged area. The snapshots in figure 1 help explain the observed trends; the examples in the first column depict the behaviour at lower D_s and the second column displays the behaviour for higher D_s. At lower values of D_s (lower release rate), the capsule moves relatively slowly (figure 3*b*) and the released particles remain fairly localized around the capsule (first column, figure 1). The motion is sufficiently slow and the particle dispersion is sufficiently localized that there is both adequate time and a sufficient number of particles to fill in sites in the vicinity of the capsule. In other words, there are enough resources to provide an effective coating.

On the other hand, when D_s is relatively high, the second column in figure 1 shows that the quicker release leads to a relatively broad particle dispersion. The particles effectively pave the way ahead of the capsule. Consequently, the capsule can move more rapidly along the surface; in particular, the attraction from the partially filled sites upstream of the capsule 'pulls' this carrier along the substrate when it reaches the damaged area. Hence, for higher values of D_s, the capsules spend less time near the damaged region, as can be clearly seen by comparing the last snapshots in the two columns. At the same instant of time, the capsule with a lower D_s is only half way through the damaged region, while the capsule with the higher D_s has already left this area. Owing to its more rapid progress, the latter capsule has less time to deliver a sufficient number of particles to each site and, consequently, the overall coverage is lower.

In the case for the lowest adhesion strength ($\Phi=2.5$), the system now shows that the surface coverage actually increases slightly with increasing D_s. Owing to the relatively weak adhesive interaction, the capsule's velocity is relatively high and is seen to be insensitive to the value of D_s (figure 3*b*). Hence, it is the particle release rate and not the capsule's velocity that dominates the behaviour of the system; the only way to localize more particles onto the damaged region from a quickly moving carrier is to increase the rate at which the particles actually leave the carrier. Consequently, increasing D_s leads to higher surface coverage.

In the final set of studies, we fix $\Phi=4.1$ and $D_s=2\times10^{-4}$, and vary D_f, the diffusion coefficient of the nanoparticles in the fluid. Since D_f is an inherent property of the nanoparticles, it is best to consider variations of D_f being equivalent to varying the Peclet number, $Pe=U_0H/D_f$. Consequently, the following discussion is phrased in terms of Pe, a dimensionless parameter that can be varied readily in an experimental study.

In figure 4, we show how the surface coverage and the capsule's relative velocity vary with increasing Pe. The images within the plot in figure 4*a* are snapshots from the simulations at identical times and serve to illustrate the behaviour at both high and low Pe. As noted earlier, a high Pe number indicates a situation where convection dominates the transport of particles away from the capsule's surface. Since the particles follow the streamlines in the fluid, with only little deviation due to diffusion, only a small fraction near the surface can adsorb onto the substrate and thus, the final mean surface coverage is low.

At low Pe, the particles can readily diffuse throughout the fluid and as seen by the image of the capsule for this range of parameters, the particle dispersion is relatively broad. Consequently, there is not only a high surface coverage in the immediate vicinity of the capsules, but also a high fraction of sites upstream of the capsule are coated or 'pre-paved'. Both the high local surface coverage and the 'pre-paving' contribute to a higher mean capsule velocity with lower Pe.

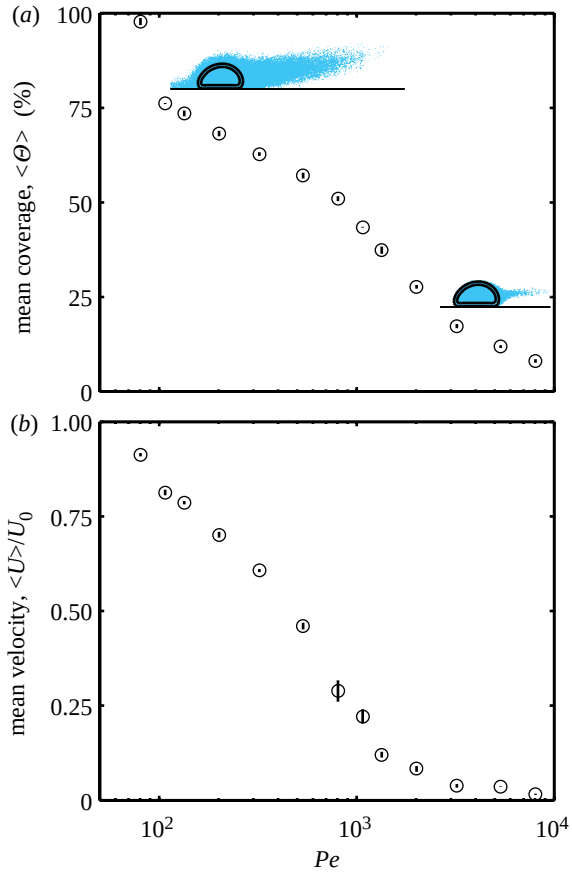

Figure 4. (*a*) Mean surface coverage, $\langle\Theta\rangle$, (in %) and (*b*) mean relative capsule velocity, $\langle U\rangle/U_0$, as a function of Pe for $\Phi=4.1$ and $D_s=2\times10^{-4}$. The data points and error bars are obtained in the same manner as shown in figure 3. The two snapshots are for identical times and serve to illustrate the behaviour at both low and high Pe.

4. CONCLUSIONS

Inspired by the behaviour of biological cells involved in wound repair, we focused on designing a synthetic system that could 'sense' the presence of a damaged surface site, localize at that site and release agents which would restore the integrity of the substrate. Polymeric microcapsules serve as our model system because they are fairly robust and can encapsulate a broad array of components. Here, the encapsulated components are taken to be nanoparticles because researchers can now produce a stunning variety of nanoparticles that display a range of surface chemistries and properties. By considering the release and diffusion of the nanoparticles from the microcapsules, and the subsequent adsorption of these species at a specific surface region, we could also obtain much needed insight into the factors that control the dispersion of the particles and thereby facilitate the design of effective microcapsules for targeted delivery.

The motion of our microcapsules is driven by an imposed flow, such as the flow that circulates species in microfluidic devices. We assume that the capsules roll on an adhesive substrate and that damage to the surface diminishes the adhesive properties of the substrate. It is through this variation in the adhesive properties that the capsule is able to 'sense' the presence of a fault in the system. The lack of a compatible coating in the damaged region can counteract the force owing to the imposed flow and arrest the motion of the capsule, localizing it at the edge of the fault. Since the capsule is trapped at the leading edge of the damaged region, a relatively high fraction of the released particles are now localized near this region and can more effectively cover these damaged sites. Once the damage is repaired, the capsule can again be driven by the imposed flow to move along the surface. Through this scenario, we have designed a biomimetic system that senses and responds to damage.

One potential route for realizing this scenario experimentally is to consider the case where the capsules and surface coating are hydrophilic and the damage has exposed an underlying hydrophobic layer. As noted earlier, ideal nanoparticles for this application could be Janus beads (Perro *et al.* 2005), or hydrophilic particles with a low surface coverage of labile hydrophobic ligands (Kim *et al.* 2006). These particles can bind to the exposed sublayer through the hydrophobic moieties, exposing a hydrophilic portion to the fluid and the capsule.

We note that the utilization of hydrophobic and hydrophilic species provides just one example of the possible chemistries that could be harnessed to produce the behaviour described earlier. To actually model this complex behaviour and establish the necessary design rules, we integrated the LBM, LSM and a Brownian dynamics model. The computational efficiency of these mesoscale models allows us to capture not only the fluid–structure interactions in the system, but also the different temporal events, i.e. the motion of the capsule and the convection and diffusion of the particles.

Through these studies, we found that the following variables have a significant effect on the behaviour of the system: the strength of the adhesive interaction between the capsule and the substrate (as measured by Φ), the rate of diffusion of the particles through the shell (D_s and consequently the release rate) and the Peclet number (Pe) of the flow. In particular, the adhesive interaction should be sufficiently strong and the difference in Φ between the undamaged and the damaged regions should be sufficiently large that the capsule is sensitive to the presence of the eroded region. The adhesive interaction can be tailored through the coating on the surface or the capsule. In addition, the value of D_s should be relatively low to provide a high surface coverage and to prevent the system from running out of particles before the capsule can reach and repair the damaged area. Finally, the Peclet number should be relatively low to prevent the particles from being swept away by the imposed flow. The value of Pe can be readily modulated in an experimental setup by changing the imposed fluid flow rate.

Since the underlying physics that controls the behaviour of this system is not dependent on the dimensionality of the system, we anticipate that we would find qualitatively similar behaviour in three-dimensional systems. Studies are currently underway to extend the current model to three dimensions; since we have already employed a three-dimensional version of our integrated 'LBM/LSM' approach (Buxton *et al.*

2005), the extension of the current model to three-dimensional can be carried out in a straightforward manner.

REFERENCES

Ai, H., Jones, S. A., de Villiers, M. M. & Lvov, Y. M. 2003 Nano-encapsulation of furosemide microcrystals for controlled drug release. *J. Control. Release* **86**, 59–68. (doi:10.1016/S0168-3659(02)00322-X)

Alexeev, A., Verberg, R. & Balazs, A. C. 2005 Modeling the motion of microcapsules on compliant polymeric surfaces. *Macromolecules* **38**, 10 244–10 260. (doi:10.1021/ma0516135)

Alexeev, A., Verberg, R. & Balazs, A. C. 2006 Designing compliant substrates to regulate the motion of vesicles. *Phys. Rev. Lett.* **96**, 148 103. (doi:10.1103/PhysRevLett.96.148103)

Ashurst, W. T. & Hoover, W. G. 1976 Microscopic fracture studies in the two-dimensional triangular lattice. *Phys. Rev. B* **14**, 1465–1473. (doi:10.1103/PhysRevB.14.1465)

Bosio, V., Dubreuil, F., Bogdanovic, G. & Fery, A. 2004 Interactions between silica surfaces coated by polyelectrolyte multilayers in aqueous environment: comparison between precursor and multilayer regime. *Colloids Surf. A Physicochem. Eng. Asp.* **243**, 147–155. (doi:10.1016/j.colsurfa.2004.06.011)

Bouzidi, M., Firdaouss, M. & Lallemand, P. 2001 Momentum transfer of a Boltzmann-lattice fluid with boundaries. *Phys. Fluids* **13**, 3452–3459. (doi:10.1063/1.1399290)

Buxton, G. A., Care, C. M. & Cleaver, D. J. 2001 A lattice spring model of heterogeneous materials with plasticity. *Model. Simulation Mater. Sci. Eng.* **9**, 485–497. (doi:10.1088/0965-0393/9/6/302)

Buxton, G. A., Verberg, R., Jasnow, D. & Balazs, A. C. 2005 Newtonian fluid meets an elastic solid: coupling lattice Boltzmann and lattice-spring models. *Phys. Rev. E* **71**, 056707. (doi:10.1103/PhysRevE.71.056707)

Donbrow, M. (ed.) 1992 *Microcapsules and nanoparticles in medicine and pharmacy*. Boca Raton, FL: CRC Press.

Dubreuil, F., Elsner, N. & Fery, A. 2003 Elastic properties of polyelectrolyte capsules studied by atomic-force microscopy and RICM. *Eur. Phys. J. E* **12**, 215–221. (doi:10.1140/epje/i2003-10056-0)

Elsner, N., Dubreuil, F. & Fery, A. 2004 Tuning of microcapsule adhesion by varying the capsule-wall thickness. *Phys. Rev. E* **69**, 031802. (doi:10.1103/PhysRevE.69.031802)

Fery, A., Dubreuil, F. & Mohwald, H. 2004 Mechanics of artificial microcapsules. *N. J. Phys.* **6**, 18. (doi:10.1088/1367-2630/6/1/018)

Kim, B. J., Bang, J., Hawker, C. J. & Kramer, E. J. 2006 Effect of areal chain density on the location of polymer-modified gold nanoparticles in a block copolymer template. *Macromolecules* **39**, 4108–4114. (doi:10.1021/ma060308w)

Nolte, M. & Fery, A. 2004 Coupling of individual polyelectrolyte capsules onto patterned substrates. *Langmuir* **20**, 2995–2998.

Ottinger, H. C. 1996 *Stochastic processes in polymeric fluids*. Berlin, Germnay: Springer.

Perro, A., Reculusa, S., Ravaine, S., Bourgeat-Lami, E. B. & Duguet, E. 2005 Design and synthesis of Janus micro- and nanoparticles. *J. Mater. Chem.* **15**, 3745–3760. (doi:10.1039/b505099e)

Skirtach, A. G., Dejugnat, C., Braun, D., Susha, A. S., Rogach, A. L., Parak, W. J., Mohwald, H. & Sukhorukov, G. B. 2005 The role of metal nanoparticles in remote release of encapsulated materials. *Nano Lett.* **5**, 1371–1377. (doi:10.1021/nl050693n)

Succi, S. 2001 *The lattice Boltzmann equation for fluid dynamics and beyond. Numerical mathematics and scientific computation*. New York, NY; Oxford, UK: Clarendon Press; Oxford University Press.

Sukhorukov, G. B. *et al.* 2005 Nanoengineered polymer capsules: tools for detection, controlled delivery, and site-specific manipulation. *Small* **1**, 194–200. (doi:10.1002/smll.200400075)

Szymczak, P. & Ladd, A. J. C. 2003 Boundary conditions for stochastic solutions of the convection-diffusion equation. *Phys. Rev. E* **68**, 036704. (doi:10.1103/PhysRevE.68.036704)

Therriault, D., Shepherd, R. F., White, S. R. & Lewis, J. A. 2005 Fugitive inks for direct-write assembly of three-dimensional microvascular networks. *Adv. Mater.* **17**, 395–399. (doi:10.1002/adma.200400481)

Tuckerman, M., Berne, B. J. & Martyna, G. J. 1992 Reversible multiple time scale molecular-dynamics. *J. Chem. Phys.* **97**, 1990–2001. (doi:10.1063/1.463137)

Verberg, R., Yeomans, J. M. & Balazs, A. C. 2005 Modeling the flow of fluid/particle mixtures in microchannels: encapsulating nanoparticles within monodisperse droplets. *J. Chem. Phys.* **123**, 224 706. (doi:10.1063/1.2133733)

Verberg, R., Alexeev, A. & Balazs, A. C. Submitted. Modeling the release of nanoparticles from mobile microcapsules. *J. Chem. Phys.*

Vinogradova, O. I. 2004 Mechanical properties of polyelectrolyte multilayer microcapsules. *J. Phys. Condensed Matter* **16**, R1105–R1134. (doi:10.1088/0953-8984/16/32/R01)

Whitesides, G. M. & Wong, A. P. 2006 The intersection of biology and materials science. *Mater. Res. Soc. Bull.* **31**, 19–27.